CHIN. PHYS. LETT. Vol. 38, No. 11 (2021) 113401

Ab Initio Study of Single- and Double-Electron Capture Processes in Collisions of He^{2+} Ions and Ne Atoms

Xiao-Xia Wang(王小霞)[1], Kun Wang(王堃)[2], Yi-Geng Peng(彭裔耕)[3], Chun-Hua Liu(刘春华)[4], Ling Liu(刘玲)[5], Yong Wu(吴勇)[5], Heinz-Peter Liebermann[6], Robert J. Buenker[6], and Yi-Zhi Qu(屈一至)[1*]

[1]*College of Material Sciences and Optoelectronic Technology, University of Chinese Academy of Sciences, Beijing 100049, China*
[2]*Institute of Environmental Science, Shanxi University, Taiyuan 030006, China*
[3]*Department of Applied Physics, Nanjing University of Science and Technology, Nanjing 210094, China*
[4]*School of Physics, Southeast University, Nanjing 210094, China*
[5]*Data Center for High Energy Density Physics, Institute of Applied Physics and Computational Mathematics, Beijing 100088, China*
[6]*Fachbereich C-Mathematik und Naturwissenschaften, Bergische Universitat Wuppertal, D-42097 Wuppertal, Germany*

(Received 2 August 2021; accepted 29 September 2021; published online 27 October 2021)

The single- and double-electron capture (SEC, DEC) processes of He^{2+} ions colliding with Ne atoms are studied by utilizing the full quantum-mechanical molecular-orbital close-coupling method. Total and state-selective SEC and DEC cross sections are presented in the energy region of 2 eV/u to 20 keV/u. Results show that the dominant reaction channel is $Ne^{+}(2s2p^6\ ^2S) + He^{+}(1s)$ in the considered energy region due to strong couplings with the initial state $Ne(2s^22p^6\ ^1S) + He^{2+}$ around the internuclear distance of 4.6 a.u. In our calculations, the SEC cross sections decrease initially and then increase whereby, the minimum point is around 0.38 keV/u with the increase of collision energies. After considering the effects of the electron translation factor (ETF), the SEC cross sections are increased by 15%–25% nearby the energy region of keV/u and agree better with the available results. The DEC cross sections are smaller than those of SEC because of the larger energy gaps and no strong couplings with the initial state. Due to the Demkov-type couplings between DEC channel $Ne^{2+}(2s^22p^4\ ^1S) + He(1s^2)$ and the dominating SEC channel $Ne^{+}(2s2p^6\ ^2S) + He^{+}(1s)$, the DEC cross sections increase with increasing impact energies. Good consistency can also be found between the present DEC and the experimental measurements in the overlapping energy region.

DOI: 10.1088/0256-307X/38/11/113401

The electron capture processes involving collisions between ions and atoms or molecules not only are of significance in fundamental atomic physics[1] but also can be directly applied to magnetic fusion plasma diagnostics for planetary research.[2] In the astronomy environment, the charge exchange in solar wind ions (e.g., H, He, C, N, O, Ne) and neutrals has contributed to understanding the processes that produce x-rays from the solar system, supernova remnant, and starburst galaxies.[3] As reported by Cravens[4] and Bochsler,[5] the abundance of helium in solar wind ions is second only to hydrogen. In addition, compared with the difficulties in the detection of neutral hydrogen the relative concentrations of He^{2+} and He^{+} can monitor the charge exchange process very accurately because no measurable He^{+} is expected from the comet.[6] Research[7] of cometary noble gas abundances and their isotopic compositions is helpful to investigate the compositional links between comets, the solar nebula, primitive meteorites and the atmospheres of Earth, Mars, and Venus. Neon[5] is an excellent tracer since the types of isotopic compositions in various solar system materials are distinctive. The composition of solar energetic particles varies significantly from event to event. In view of data completeness in spectral modeling tools, details of the collisions of He^{2+} ions with Ne atoms are very necessary for modelers.

Many earlier works have studied the charge exchange process by the He^{2+}–Ne collisions. For the experimental work, e.g., Rudd *et al.*,[8] Dubois *et al.*[9,10] and Baragiola *et al.*,[11] have measured the electron capture and ionization cross sections of He^{2+}–Ne in the energy range above 5 keV/u. Afrosimov *et al.*[12] observed the single-electron capture processes in the impact energies of 0.68–10 keV/u. Hanaki *et al.*[13] measured the single- and double-electron capture (SEC, DEC) of He^{2+} from Ne gas targets in the energy range of 0.7–4.5 keV (0.18–1.13 keV/u). In 2007, Abdelrahman and co-workers[14] observed the

Supported by the National Natural Science Foundation of China (Grant Nos. 11774344 and 11474033), and the National Key Research and Development Program of China (Grant No. 2017YFA0402300).
*Corresponding author. Email: yzqu@ucas.ac.cn
© 2021 Chinese Physical Society and IOP Publishing Ltd

total cross sections for SEC in He^{2+}–Ne collisions in the 260–2000 eV (0.065–0.5 keV/u). During the same year, the absolute cross sections for SEC and DEC in collisions energies of 0.1–10 keV (0.025–2.5 keV/u) for He^{2+}–Ne were given by Silva *et al.*[15] For the theoretical aspect, Afrosimov *et al.*[16] and Kirchner *et al.*[17,18] have investigated the total and multiple cross sections of electron capture, loss and ionization by the continuum distorted-wave (CDW) approximation and the basis generator method (BGM) above 10 keV/u. Hong *et al.*[19] calculated the SEC and DEC based on the time-dependent density functional theory (TDDFT) in the energy range of 1–1000 keV/u. As the impact energies above 1.0 keV/u, the available theoretical data agree well with the experimental results. However, when the impact energies are below 0.5 keV/u, obvious discrepancies remain in the experimental data of Silva *et al.*[15] and Abdelrahman *et al.*[14] One increases with the increasing impact energies but the other one decreases. Though the Landau–Zener theory (LZ) results of Abdelrahman *et al.*[14] also have a falling trend, the data are about 2–3 times larger than in the measurements. More investigations are expected for the He^{2+} and Ne collisions.

In this Letter, the full quantum-mechanical molecular-orbital close-coupling (QMOCC) method[20,21] is used to study the electron capture processes by the He^{2+} and Ne collisions in the energy region of 2 eV/u to 20 keV/u. The QMOCC could accurately deal with the correlation effect among electrons and nucleus in the collisions between low-energy ions and atoms,[22,23] which has been developed to treat systems with higher precisions,[24] more electrons and states (even pseudo-states)[25,26] as well as more complex reactions (dissociation and dissociative capture processes, and so on)[27] with the development of the computing capacity and technology. The corresponding electronic structures (potential energies, radial and rotational coupling matrices) needed in the dynamics are calculated from the multi-reference single- and double-excitation configuration interaction (MRDCI) package.[28,29] With this calculation, the discrepancies of the experimental measurements[14,15] are clarified in the low-energy region. The present dominant electron capture channel with an exothermic energy defect of about 5.9 eV with the initial state is consistent with the experimental conclusion of Abdelrahman *et al.*,[14] Silva *et al.*[15] and Austin *et al.*[30] Atomic units are used throughout unless otherwise stated.

The electron capture cross sections for He^{2+}–Ne collision are performed by the QMOCC method. This method has been described in detail in the literature.[21,31] In the perturbed stationary state model (PSS),[20–22] after expanding the total wave functions by adiabatic electric wave functions, the radial function satisfies a set of second-order differential equations, in which the radial and rotational coupling matrices A^R_{ij} and A^c_{ij} connect the adiabatic states with the same and different symmetry and cause transitions between them. For numerical convenience, a unitary transformation of the adiabatic representation is made to an adiabatic one. In the diabatic potentials and couplings, the coupled set of second-order differential equations is solved by the multichannel log-derivative algorithm of Johnson.[32] By matching the plane-wave boundary conditions at a large nuclear separation, the K matrix is obtained and the S matrix can be written as

$$S_J = \frac{I + iK_J}{I - iK_J}, \tag{1}$$

where I represents the unit matrix and J is the partial wave. Then the cross section σ for states i to j can be defined as

$$\sigma_{(i\to j)} = \frac{\pi}{k_i^2}\sum_J (2J+1)|S_J|^2_{i,j}, \tag{2}$$

with k_i being the initial momentum in the center-of-mass coordinate.

In the QMOCC calculations, the effects of electron translation factor (ETF) were made by choosing the reaction coordinates and switching function from Gargaud,[33] which is identical to the semi-classical CTF adopted by Errea,[34] the radial and rotational interaction can be replaced by[35]

$$\begin{aligned} &\left\langle \psi_i|\partial/\partial R - (\varepsilon_i - \varepsilon_j)z^2/2R|\psi_j\right\rangle, \\ &\left\langle \psi_i|iL_y + (\varepsilon_i - \varepsilon_j)zx|\psi_j\right\rangle, \end{aligned} \tag{3}$$

where R is the internuclear distance, L_y is the component of the electronic angular momentum, z^2 and zx are the components of the quadrupole moment tensor, ε_i and ε_j are the electronic energies of states ψ_i and ψ_j.

The adiabatic potential energies of the $HeNe^{2+}$ system are obtained from the MRDCI package in the region of 1.0 to 50.0 a.u. In this calculation, the lowest nineteen molecular states: eight $^1\Sigma^+$, four $^1\Delta$ (A_1 symmetry) and seven $^1\Pi$ (B_1 symmetry) are included. For neon atoms, the effective core potential (ECP)[36] and the Aug-cc-pVQZ (augmented correlation consistent polarization valence quadruple ζ) basis[37] diffused by a set of $(1s,1p)$ functions are employed, i.e., $(14s,8p,3d,2f)$ contracted to $[7s,6p,3d,2f]$. The basis set of $(7s3p)/[5s3p]$ of Romelt *et al.*[38] by adding a d-type function for He is used here. The g functions are discarded and the spin-orbit interactions are not considered for their small effects. The asymptotic atomic energies corresponding to the molecular states for $HeNe^{2+}$ are listed in Table 1 and compared with the experimental results.[39] Except for the initial state $7^1\Sigma^+$ asymptotically corresponding to the $Ne(2s^22p^6\ ^1S) + He^{2+}$ atomic state, i.e., $[Ne(^1S) + He^{2+};\ 7^1\Sigma^+]$,

the differences between our calculation and the experimental data are below 0.1 eV in the asymptotic region.

The adiabatic potential curves of the nineteen molecular states above are plotted in Fig. 1 ranged from 1.0 a.u. to 20.0 a.u., the lowest two states $[Ne^+(^2P^o) + He^+;\ 1^1\Sigma^+$ and $1^1\Pi]$ are partly shown for their energies are about 30 eV lower than the entrance channel. Besides, two sharp avoided crossings, between $[Ne^+(^2D) + He^+;\ 5^1\Sigma^+]$, $[Ne^+(^2P^o) + He^+;\ 6^1\Sigma^+]$ and initial state $[Ne(^1S) + He^{2+};\ 7^1\Sigma^+]$ around 10.6 a.u. and 18.4 a.u., have been treated diabatically. From Fig. 1, it is known that a strong crossing exists between the initial state $[Ne(^1S) + He^{2+};\ 7^1\Sigma^+]$ and $[Ne^+(^2S) + He^+;\ 4^1\Sigma^+]$ at internuclear distance about 4.6 a.u., which will play a crucial role in the low-energy collision dynamics. Strong avoided crossing can also be found between initial state $[Ne(^1S) + He^{2+};\ 7^1\Sigma^+]$ and $[Ne^+(^2D) + He^+;\ 5^1\Sigma^+]$ as well as $[Ne^+(^2P^o) + He^+;\ 6^1\Sigma^+]$ and $[Ne^+(^2D) + He^+;\ 5^1\Sigma^+]$ at internuclear distance around 2.3 a.u. and 4.0 a.u., respectively, which will be important for SEC process if enough impact energies are reached. With the reducing internuclear distances R, the single-electron capture (SEC) channel $[Ne^+(^2S) + He^+;\ 4^1\Sigma^+]$ and the double-electron capture (DEC) channel $[Ne^{2+}(^1S) + He;\ 3^1\Sigma^+]$ begin to approach each other. It is suggested that the electron can flux between the two states by the Demkov-type mechanism,[40,41] which would be the main gateway of electron capture to the DEC channels. Furthermore, compared with the DEC channels $[Ne^{2+}(^1D) + He;\ 2^1\Sigma^+,\ 2^1\Pi$ and $1^1\Delta]$ and $[Ne^{2+}(^1S) + He;\ 3^1\Sigma^+]$, the SEC channels, e.g., $[Ne^+(^2S) + He^+;\ 4^1\Sigma^+]$, $[Ne^+(^2D) + He^+;\ 5^1\Sigma^+,\ 4^1\Pi$ and $2^1\Delta]$ and $[Ne^+(^2D^o) + He^+;\ 5^1\Pi$ and $3^1\Delta]$, are energetically closer to the initial state. It can be deduced that the SEC should be the dominant electron capture processes in the low energy region.

Table 1. Asymptotic atomic energies for the $HeNe^{2+}$ molecular ions.

Molecular states	Asymptotic atomic states	Energy and error (eV)		
		NIST	MRDCI	Error
$1^1\Sigma^+,\ 1^1\Pi$	$Ne^+(2s^22p^5\ ^2P^o) + He^+(1s)$	0	0	0
$2^1\Sigma^+,\ 2^1\Pi,\ 1^1\Delta$	$Ne^{2+}(2s^22p^4\ ^1D) + He(1s^2)$	19.579	19.665	0.086
$3^1\Sigma^+$	$Ne^{2+}(2s^22p^4\ ^1S) + He(1s^2)$	23.288	23.207	0.080
$4^1\Sigma^+$	$Ne^+(2s2p^6\ ^2S) + He^+(1s)$	26.910	26.872	−0.038
$3^1\Pi$	$Ne^+(2s2p^43s\ ^2P) + He^+(1s)$	27.783	27.790	0.007
$5^1\Sigma^+,\ 4^1\Pi,\ 2^1\Delta$	$Ne^+(2s^22p^43s\ ^2D) + He^+(1s)$	30.549	30.533	−0.016
$5^1\Pi,\ 3^1\Delta$	$Ne^+(2s^22p^43p\ ^2D^o) + He^+(1s)$	31.121	31.076	−0.045
$6^1\Sigma^+,\ 6^1\Pi$	$Ne^+(2s^22p^43p\ ^2P^o) + He^+(1s)$	31.512	31.453	−0.059
$7^1\Sigma^+$	$Ne(2s^22p^6\ ^1S) + He^{2+}$	32.853	33.018	0.165
$8^1\Sigma^+,\ 7^1\Pi,\ 4^1\Delta$	$Ne^+(2s^22p^43p\ ^2F^o) + He^+(1s)$	34.017	34.096	0.079

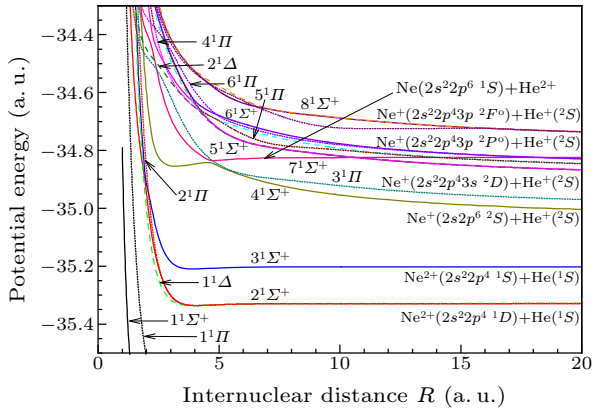

Fig. 1. Adiabatic potential curves of $HeNe^{2+}$. The solid lines, dotted lines and dashed lines represent the $^1\Sigma^+$, $^1\Pi$ and $^1\Delta$ states, respectively.

The radial and rotational coupling matrix elements represent the couplings between the states in identical or different symmetry. Some important radial coupling matrix elements of $^1\Sigma^+$ and $^1\Pi$ states calculated from the finite-difference approximation are shown in Fig. 2 by considering the ETF effects.[34] There is almost a one-to-one correlation between the position of a peak in the radial couplings and an avoided crossing of the adiabatic potentials in Fig. 1. As the internuclear distances $R > 3.0$ a.u. in Fig. 2(a), a strong peak centered around 4.6 a.u. appears between the $4^1\Sigma^+$ state and the initial state $7^1\Sigma^+$. This interaction contributes to the main electron capture in the low-energy collision. As the internuclear distance R decreases, the couplings of $4^1\Sigma^+$–$7^1\Sigma^+$ approach zero until $R \sim 1.8$ a.u. The obvious strong couplings can also be found between $5^1\Sigma^+$ and $7^1\Sigma^+$ in internuclear distance about 2.30 a.u., 1.67 a.u. and 1.40 a.u., which will be crucial to the SEC process as impact energies increase. As the states $6^1\Sigma^+$ and $8^1\Sigma^+$ are adjacent to the initial state $7^1\Sigma^+$, the typically Demkov-type couplings featured with the broad and shallow peaks appear between them nearly 1.8 a.u. Similarly, the coupling between $3^1\Sigma^+$ and $4^1\Sigma^+$ can also be classified to the Demkov-type, which is responsible for the population of the double-electron capture channel.

The electrons transferred between states of different symmetry are driven by rotational couplings.

Some typical rotational coupling matrix elements are displayed in Fig. 3. These curves are not smooth as the radical near the positions of avoided crossings, because of the strong adiabatic interactions between the adjacent states. As displayed in Fig. 3(a), compared with the couplings between the same atomic configurations, e.g., $1^1\Sigma^+ - 1^1\Pi$ and $6^1\Sigma^+ - 6^1\Pi$, the couplings between the different atomic configurations states are much weaker and reduce to zero in the region of $R > 5.0$ a.u. In this system, the rotational couplings tend to redistribute the populations between states with the same configurations. Since there are no $^1\Sigma^+$ states with the same configurations with $3^1\Pi$ and $5^1\Pi$, which contribute to the population of $Ne^+(^2P) + He^+$ and $Ne^+(^2D^o) + He^+$ exit channels, three prominent rotational coupling matrix elements between $^1\Sigma^+$ and $3^1\Pi/5^1\Pi$ are displayed in Fig. 3(b). The broad coupling curves between $^1\Sigma^+$ and $3^1\Pi/5^1\Pi$ around 8.0 a.u. will guarantee a certain amount of electron flux in the low-energy collision.

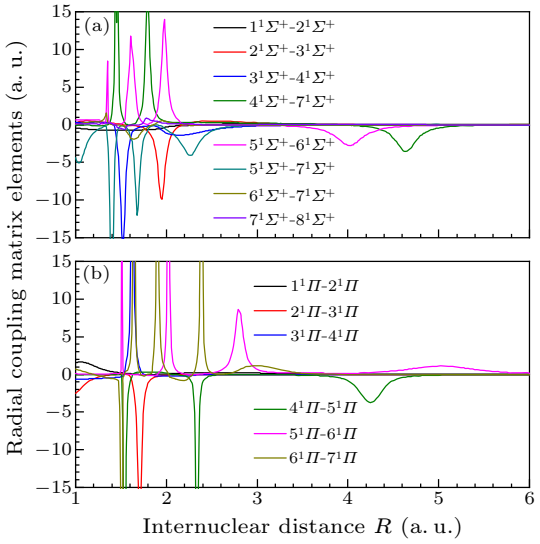

Fig. 2. Some important radial coupling matrix elements (a) for $^1\Sigma^+$ states and (b) for $^1\Pi$ states.

The present QMOCC total single- and double-electron capture cross section of the He^{2+}–Ne collision system is displayed in Fig. 4 in the energy region from 2 eV/u to 20 keV/, and compared with the available experimental and other theoretical results. For the SEC cross sections in Fig. 4(a), it is clear that the results above 1.0 keV/u can be explained well with the existing theoretical work of TDDFT and the SEC cross sections from QMOCC can smoothly connect with the TDDFT results of Hong *et al.*[19] at 1.0 keV/u. In our calculations, the ETF effects contribute largely to the SEC cross sections, which are enhanced by 15%–25% as the collision energies $E > 0.5$ keV/u, e.g., the cross section is increased from 2.95 to 3.61 $\times 10^{-16}$ cm^2 at collision energy of 1.2 keV/u. In this energy region, the present data are less than 1.0 $\times 10^{-16}$ cm^2 larger than the measurements of Hanaki *et al.*[13] and Silva *et al.*[15] as well as lower than the results of Afrosimov *et al.*,[12] but lie between them in the overlapping energy region. In several keV/u, the present SEC cross sections lie between the measurements of Rudd *et al.*[8] and Baragiola *et al.*[11]

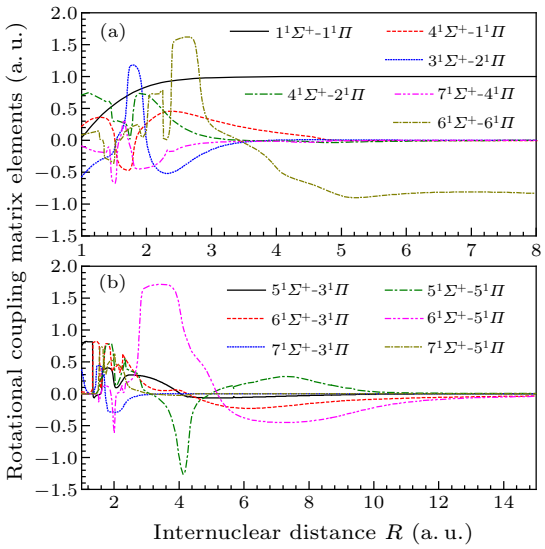

Fig. 3. Some typical rotational coupling matrix elements between $^1\Sigma^+$ and $^1\Pi$ states for $HeNe^{2+}$ (a) for $1^1\Pi$, $2^1\Pi$, $4^1\Pi$ and $6^1\Pi$ states, (b) for $3^1\Pi$ and $5^1\Pi$ states.

While below the impact energy of 0.5 keV/u, the measurements of Silva *et al.*[15] and Abdelrahman *et al.*[14] are under debate due to the opposite tendency. The Landau–Zener theory (LZ) results are characterized by a similar downtrend with the measurements of Abdelrahman *et al.*,[14] but are about 2–3 times larger in quantitative values. In this work, a valley of present SEC cross sections is formed at around 0.38 keV/u, which locate in the region of 0.2–0.5 keV/u, where the observations of Abdelrahman *et al.*[14] are minimal. Even for the differences of around 1.0 $\times 10^{-16}$ cm^2, which existed between the present data and measurements, as far as known, the valley appears in theoretical works for the first time in the collision of He^{2+} and Ne. When the collision energies are below 0.38 keV/u, the SEC cross sections increase with decreasing impact energies, which support the measurements of Abdelrahman *et al.*[14] as well as the LZ method in trend. The present results are within the error range of measurements of Abdelrahman *et al.*[14] at impact energies of 66 and 100 eV/u. Compared with the LZ method, the SEC cross sections of the QMOCC are closer to the observations, for instance, at energy of 0.25 keV/u, the results of QMOCC and LZ are about 1.0 and 2.5 $\times 10^{-16}$ cm^2 higher than the measurement, respectively. With the reduction of impact energies, the differences of SEC cross sections between the QMOCC and LZ are increased, which

are even larger than $4 \times 10^{-16}\,\mathrm{cm}^2$ at some energy points. In the low-energy region, the QMOCC methods are more reliable due to the fact that $HeNe^{2+}$ may stay in the molecular region for a longer time and the quasimolecule treatment of present QMOCC is sufficient to perform the interactions between ions and atoms.[42] The disagreement between the measurements of Silva *et al.*[15] and Abdelrahman *et al.*[14] may result from the data processing. In their experiments, the attenuation method was used for determining the electron capture cross sections. The differences are that in the measurements of Silva *et al.*,[15] the attenuated cross sections are composed of SEC, DEC and transfer ionization, and the SEC cross sections are obtained by subtracting the transfer ionization. As described by Lin,[43] at low energies, the excitation or ionization processes are very weak to compete with the strong transfer channels. The underestimate of about $1.0 \times 10^{-16}\,\mathrm{cm}^2$ between the measurement of Abdelrahman *et al.*[14] and present QMOCC from 0.1 to 1 keV/u may ascribe to the influence of metastable fraction, contamination from ions with the same charge/mass ratio of the ion beam, or insufficient collection in scattering processes. Some further measurements should help clarify the discrepancy.

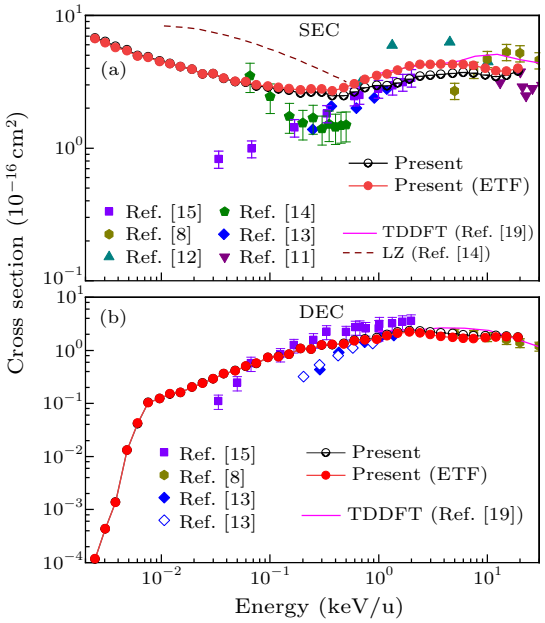

Fig. 4. Comparisons of the present QMOCC electron capture cross sections with other experimental and theoretical results. Theory: the present QMOCC (solid line with circle), the time-dependent density functional theory (TDDFT) results of Hong *et al.*[19] (solid line), the Landau–Zener theory (LZ) results of Abdelrahman *et al.*[14] (dashed line); experiment: Silva *et al.*[15] (full square), Abdelrahman *et al.*[14] (full pentagon), Rudd *et al.*[8] (full hexagon), Hanaki *et al.*[13] (diamond), Baragiola *et al.*[11] (inverted full triangle), Afrosimov *et al.*[12] (full triangle). (a) For SEC cross sections, and (b) for DEC cross sections.

The DEC cross sections of the He^{2+}–Ne collision are displayed in Fig. 4(b). On the whole, the present DEC are smaller than the SEC process and are increased with increasing impact energies. These features will be explained in the state-selective cross sections part. As the impact energies $E < 66$ eV/u, the measurement of Silva *et al.*[15] are smaller than our calculations. This underestimate may be the result of insufficient collection due to angular scattering effects in the low-energy collision. In the energy region of 66–250 eV/u, the present DEC cross sections are in good agreement with Silva *et al.*[15] and about $0.7 \times 10^{-16}\,\mathrm{cm}^2$ larger than measurements of Hanaki *et al.*[13] With the increasing of impact energies, the experimental measurements of Silva *et al.*[15] and Hanaki *et al.*[13] successively approach each other and the present DEC cross sections lie between them in the overlapping energy region. Similar to the SEC cross section, the present DEC can connect well with the results of Hong *et al.*[19] In several keV/u, good agreement can be found between the present data and the experimental measurements of Rudd *et al.*[8] By taking the effect of ETF into account, the DEC cross sections are reduced with differences below 15%, e.g., from $2.06 \times 10^{-16}\,\mathrm{cm}^2$ to $1.75 \times 10^{-16}\,\mathrm{cm}^2$ at 4.8 keV/u.

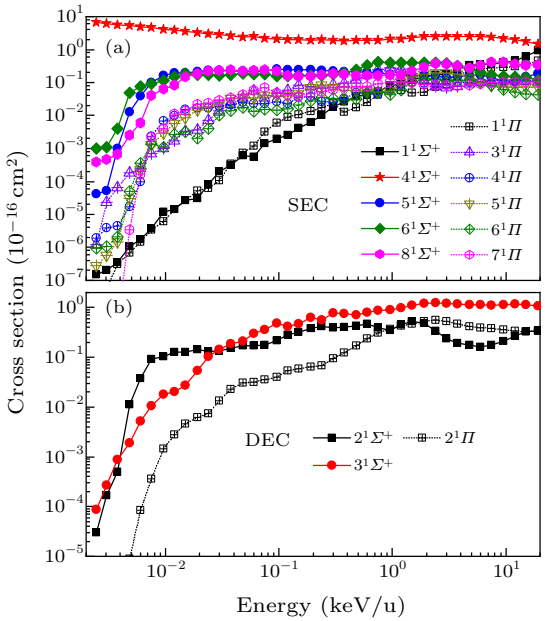

Fig. 5. State-selective cross section from initial state $[\mathrm{Ne}(^1S) + \mathrm{He}^{2+};\ 7^1\Sigma^+]$ to other states with considering ETF effects. $^1\Sigma^+$ states: solid lines with filled symbols; $^1\Pi$ states: dotted lines with open symbols. (a) For SEC cross sections, and (b) for DEC cross sections.

To study the electron capture cross sections in detail, the state-selective cross sections of SEC and DEC are displayed in Fig. 5. As shown in Fig. 5(a), the SEC channels can be classified into four groups according to the contribution to the total SEC cross sections. Firstly, due to the strong interactions between the initial state $[\mathrm{Ne}(^1S) + \mathrm{He}^{2+};\ 7^1\Sigma^+]$ and $[\mathrm{Ne}^+(^2S) + \mathrm{He}^+;$

$4^1\Sigma^+$] around 1.8 a.u. and 4.6 a.u., the characteristic of the SEC cross sections is dominantly determined by the electron exchange between the $7^1\Sigma^+$ and $4^1\Sigma^+$ states. As the increasing of impact energies, the SEC cross sections decrease firstly and subsequently increase. This feature can be explained by the classical turning point, which moves to the smaller internuclear distance as the increase of impact energies. For no noteworthy couplings between $7^1\Sigma^+$ and $4^1\Sigma^+$ in the region of 2.0–4.0 a.u., the SEC cross sections are minimized around the energy of 0.38 keV/u. Secondly, because the obvious couplings between $5^1\Sigma^+$ and $7^1\Sigma^+$ about 2.30 a.u. and the Demkov-type couplings in $6^1\Sigma^+ - 7^1\Sigma^+$ and $8^1\Sigma^+ - 7^1\Sigma^+$, the contributions from the adjacent states $5^1\Sigma^+$, $6^1\Sigma^+$ and $8^1\Sigma^+$ are about one order of magnitude smaller than those of $4^1\Sigma^+$, respectively. Thirdly, because of no prominent rotational couplings in this system, the SEC cross sections from $^1\Pi$ states are smaller than those of the second groups. The main effect of the rotational couplings is to redistribute the cross sections between states with the same configurations. As displayed in Fig. 3(b), the relatively broad couplings between $^1\Sigma^+$ and $3^1\Pi/5^1\Pi$ are enough to ensure the magnitude of cross sections. Lastly, the results of the states $1^1\Sigma^+$ and $1^1\Pi$ are the lowest in the low-energy region, since the large energy gaps between $1^1\Sigma^+/1^1\Pi$ and the entrance channel $7^1\Sigma^+$. With the increasing collision energy, the classical turning point moves to the smaller internuclear distance, the number of channels needed in calculations is increased dramatically in the small R region. When the impact energies are higher than 20 keV/u, the state-selective cross sections from $1^1\Sigma^+$ may exceed the $4^1\Sigma^+$ state, but this conclusion should be certified by specialized calculations in their valid energy region.

Figure 5(b) gives the state-selective cross sections for initial state $7^1\Sigma^+$ to the DEC channels. Different from the SEC channels, no obvious couplings appear between the entrance channel and the DEC in the large R region, thus the state-selective DEC cross section increases with the increasing energy duo to the Demkov-type couplings. In the beginning, the contributions from $2^1\Sigma^+$ and $3^1\Sigma^+$ are close to each other. However, because of the Demkov-type couplings between $3^1\Sigma^+$ and $4^1\Sigma^+$ nearby 2.2 a.u., the DEC cross sections of $3^1\Sigma^+$ become 2–3 times larger than those of $2^1\Sigma^+$ with increasing impact energies. The reduction of the DEC cross sections around 7.5 keV/u is mainly the result of the contributions from the $2^1\Sigma^+$ state. Similarly, the cross sections of $2^1\Pi$ are also smaller due to the weak rotational couplings with other $^1\Sigma^+$ states.

In summary, the total and state-selective SEC/DEC cross sections in the collisions of He^{2+}–Ne are performed by the QMOCC method in the energy range of 2–20 keV/u. Electronic structures of eight $^1\Sigma^+$, four $^1\Delta$ and seven $^1\Pi$ are calculated by the *ab initio* MRDCI package. In addition, two high energy states (one $^1\Sigma^+$ and one $^1\Pi$ states with asymptotic energies close to the $8^1\Sigma^+$) are added to check the convergence of our considered channels, the good agreement proves that the states whose energy are higher than the $8^1\Sigma^+$ state in the asymptotic region can be ignored in our calculations. Because of the strong interactions between the initial state $7^1\Sigma^+$ and $4^1\Sigma^+$, the $4^1\Sigma^+$ is the dominant SEC channel. That is, after collision with He^{2+} ions the Ne prefers to be in the $Ne^+(2s2p^6\ ^2S)$ state. Although the present data are about 1.0×10^{-16} cm^2 larger than the measurements of Abdelrahman *et al.*,[14] the present SEC cross sections support the falling trend below the energy of about 0.5 keV/u. When the collision energies are above 0.5 keV/u, the ETF effects can increase the SEC cross sections by 15%–25%, which are in accord with the TDDFT results of Hong *et al.*[19] In several keV/u, the present SEC cross sections are lower than the data of Hong *et al.*[19] while lie between the measurements of Rudd *et al.*[8] and Baragiola *et al.*[11] Generally, the DEC cross sections are smaller than those of SEC as larger energy gaps and no strong couplings with the initial state. The present DEC cross sections lie between the experimental data of Silva *et al.*[15] and Hanaki *et al.*[13] in the overlapping energy region. Similarly, the present DEC is around 20% smaller than the results of Hong *et al.*, but in good agreement with the experimental measurements of Rudd *et al.*[8] in the region of several keV/u.

References

[1] Gao Y, Zhu X L, Zhang S F, Zhang R T, Feng W T, Guo D L, Li B, Zhao D M, Wang H B, Huang Z K, Yan S C, Qian D B and Ma X W 2016 *Chin. Phys. Lett.* **33** 073401
[2] Otranto S, Olson R E and Beiersdorfer P 2007 *J. Phys. B* **40** 1755
[3] Bhardwaj A, Elsner R F, Randall G G, Cravens T E, Lisse C M, Dennerl K, Branduardi-Raymont G, Wargelin B J, Hunter W J, Robertson I, Østgaard N, Beiersdorfer P, Snowden S L and Kharchenko V 2007 *Planet. Space Sci.* **55** 1135
[4] Cravens T E 1997 *Geophys. Res. Lett.* **24** 105
[5] Bochsler P 1987 *Phys. Scr.* **T18** 55
[6] Shelley E G, Fuselier S A, Balsiger H, Drake J F, Geiss J, Goldstein B E, Goldstein R, Ip W H, Lazarus A J and Neugebauer M 1987 *Astron. Astrophys.* **187** 304
[7] Owen T, Bar-Nun A and Kleinfeld I 1992 *Nature* **358** 43
[8] Rudd M E, Goffe T V and Itoh A 1985 *Phys. Rev. A* **32** 2128
[9] DuBois R D 1986 *Phys. Rev. A* **33** 1595
[10] DuBois R D 1987 *Phys. Rev. A* **36** 2585
[11] Baragiola R A, Nemirovsky I B and M 1973 *Nucl. Instrum. Methods* **110** 511
[12] Afrosimov V V, Basalaev A A, Leiko G A and Panov M N 1979 *Electronic and Atomic Collisions (XI-th ICPEAC Abstracts of Contributed Papers)* 29 August–4 September, 1979, Kyoto p 580

[13] Hanaki H, Toshio K, Nobuo N and Masakatsu S 1983 *J. Phys. Soc. Jpn.* **52** 424
[14] Abdelrahman M M, Figuera D S S, Aumayr F and Winter H 2007 *6th Conference on Nuclear and Particle Physics* 17–21 November 2007, Luxor, pp 617–627
[15] Silva S F, Kowarik G, Aumayr F and Winter H 2007 *J. Phys.: Conf. Ser.* **58** 181
[16] Afrosimov V V, Barash D F, Basalaev A A, Gushchina N A, Lozhkin K O, Nikulin V K, Panov M N and Stepanov I Y 1993 *J. Exp. Theor. Phys.* **77** 554
[17] Kirchner T, Gulyás L, Lüdde H J, Engel E and Dreizler R M 1998 *Phys. Rev. A* **58** 2063
[18] Kirchner T, Horbatsch M, Lüdde H J and Dreizler R M 2000 *Phys. Rev. A* **62** 042704
[19] Hong X, Wang F, Jiao Y, Su W, Wang J and Gou B 2013 *J. Chem. Phys.* **139** 084321
[20] Bransden B H and McDowell M R C 1992 *Charge Exchange and the Theory of Ion-Atom Collision* (Oxford: Clarendon Press) p 300
[21] Zygelman B, Cooper D L, Ford M J, Dalgarno A, Gerratt J and Raimondi M 1992 *Phys. Rev. A* **46** 3846
[22] Heil T G, Butler S E and Dalgarno A 1981 *Phys. Rev. A* **23** 1100
[23] Wang K, Wang X X, Qu Y Z, Liu C H, Liu L, Wu Y and Buenker R J 2020 *Chin. Phys. Lett.* **37** 023401
[24] Liu C H, Wang J G and Janev R K 2012 *J. Phys. B* **45** 235203
[25] Zhao L B, Watanabe A, Stancil P C and Kimura M 2007 *Phys. Rev. A* **76** 022701
[26] Wang K, Qu Y Z, Liu C H, Liu L, Wu Y, Liebermann H P and Buenker R J 2019 *J. Phys. B* **52** 075202
[27] Liu C H, Wang J G and Janev R K 2014 *Phys. Rev. A* **89** 062719
[28] Krebs S and Buenker R J 1995 *J. Chem. Phys.* **103** 5613
[29] Buenker R J and Phillips R A 1985 *J. Mol. Struct.: THEOCHEM* **123** 291
[30] Austin T M, Mullen J M and Bailey T L 1975 *Chem. Phys.* **10** 117
[31] Kimura M and Lane N F 1989 *Adv. At. Mol. Opt. Phys.* **26** 79
[32] Johnson B R 1973 *J. Comput. Phys.* **13** 445
[33] Gargaud M, Mccarroll R and Valiron P 1987 *J. Phys. B* **20** 1555
[34] Errea L F, Mendez L and Riera A 1982 *J. Phys. B* **15** 101
[35] Bacchus-Montabonel M C and Ceyzeriat P 1998 *Phys. Rev. A* **58** 1162
[36] Fernandez P L and Christiansen P A 1985 *J. Chem. Phys.* **82** 2664
[37] Dunning T H 1989 *J. Chem. Phys.* **90** 1007
[38] Römelt J, Peyerimhoff S D and Buenker R J 1978 *Chem. Phys.* **34** 403
[39] Kramida A, Ralchenko Yu, Reader J and NIST ASD Team 2019 *NIST Atomic Spectra Database* (National Institute of Standards and Technology, Gaithersburg, MD)
[40] Kimura M and Lane N F 1990 *Phys. Rev. A* **41** 5938
[41] Liu C H, Liu L, Qu Y Z, Wang J G and Janev R K 2010 *Phys. Rev. A* **82** 022710
[42] Liu L, Li X Y, Wang J G and Janev R K 2014 *Phys. Plasmas* **21** 062513
[43] Fritsch W and Lin C D 1991 *Phys. Rep.* **202** 1